Catalysis Today 145 (2009) 101–107

Contents lists available at ScienceDirect

Catalysis Today

journal homepage: www.elsevier.com/locate/cattod

A FTIR and TPD examination of the distributive properties of acid sites on ZSM-5 zeolite with pyridine as a probe molecule

Fang Jin, Yongdan Li *

Tianjin Key Laboratory of Applied Catalysis Science and Technology, School of Chemical Engineering, Tianjin University, Tianjin 300072, China

ARTICLE INFO

Article history:
Available online 21 July 2008

Keywords:
Fourier transmission infrared spectroscopy
Temperature programmed desorption
Pyridines
Zeolite
ZSM-5

ABSTRACT

The amount, type, origin and strength distribution of acid sites on ZSM-5 zeolite were analyzed with pyridine as a probe molecule, and with the aid of FTIR and interrupted-temperature programmed desorption techniques. Desorption activation energy (DAE) was used as a measure of the acid strength. The acid sites were divided into four sets each with a mean strength of DAE 70, 90, 120 and 150 kJ mol^{-1}. Brönsted (B) sites were found dominant in the set with DAE 150 kJ mol^{-1}, while Lewis (L) sites prevail for the DAE 120 kJ mol^{-1} set. For the other two sets both B and L sites are important. The B sites with DAE 70 kJ mol^{-1} were attributed to terminal silanol groups, and the B sites with DAE 90 kJ mol^{-1} were due to bridged hydroxyl and extraframework AlOH groups.

1. Introduction

Characterization and measurement of acidity of zeolites, such as amount, type, origin and strength of acid sites, are important because the major applications of zeolites in commercial catalytic processes, such as fluidized catalytic cracking (Y and USY) [1], hydrocracking (Y) [2,3], dewaxing (ZSM-5, erionite, mordenite, ZSM-23) [4–6], paraffin isomerization (erioite, ZSM-5) [7–9], paraffin/olefin alkylation (Y, beta) [10], methanol to gasoline and olefins (ZSM-5) [11,12], ethylbenzene production (ZSM-5) [13], toluene disproportionation and xylene isomerization (ZSM-5) [14,15], aromatics hydrogenation (USY, MCM-41) [16–19], and Chichibabin condensation (ZSM-5) [20,21], are based on the acidic properties.

A stable and selective catalyst for Chichibabin condensation of aldehydes and ammonia to produce pyridine bases, key intermediates for pharmaceuticals, agricultural, and other fine chemicals, becomes a challenge to catalysts designers in recent years. ZSM-5 zeolite has intrinsic acidity, three-dimensional porosity, high thermal stability, and therefore, has been explored extensively as the catalyst precursor for the reaction. The condensation reaction is typically a solid acid catalyzed one, particularly with ammonia as one of the reactants and pyridine as one of the products, these are used as the probe molecules for the characterization of the acidic properties of solid catalysts in TPD and FTIR techniques. Many qualitative remarks on the effect of acidity on the performance of ZSM-5 have been proposed [20,21]. However, a quantitative relationship is needed and therefore a detailed analysis of the acid sites is helpful.

The information on the amount and strength distribution of the solid acid sites can be derived from a TPD spectrum. Nevertheless, the extraction of quantitative information in an explicit form depends on a valid interpretation of the spectrum. An early quantitative work on the thermodesorption of a gas from an energetically homogeneous surface was done in 1958 by Smith and Anoff [22]. In 1967 Cvetanović and Amenomiya [23] developed a model for the TPD process with assumptions similar to Langmuir, that the surface is energetically homogeneous and the read-sorption and intraparticle diffusion resistance are absent. The model was discussed and extended afterwards by many authors [24–30]. Bhatia et al. [31] published an excellent review on this topic. Many experimental methods were developed also to estimate the kinetic parameters such as enthalpy and desorption activation energy (DAE) [28,32–35]. Niwa and coworkers [36,37] employed a one-point method and a curve-fitting method to determine the ammonia DAE. Hashimoto et al. [38] used an interrupted-temperature programmed desorption (ITPD) method to describe the acid strength distribution.

TPD technique cannot distinguish Brönsted (B) and Lewis (L) sites. FTIR spectroscopy can be employed to discriminate the states of hydroxyl groups and to identify the types of acid sites by recognizing the adsorption bonds formed between the site and a

* Corresponding author. Tel.: +86 22 27405613; fax: +86 22 27405243.
E-mail address: ydli@tju.edu.cn (Y.D. Li).

0920-5861/$ – see front matter © 2008 Elsevier B.V. All rights reserved.
doi:10.1016/j.cattod.2008.06.007

probe molecule. However, it gives only a comparative measure of the amount of the two kinds of sites. Many works combined the two techniques to provide a comprehensive information [39–42].

In this work, FTIR and TPD techniques were employed to elucidate the acidity of ZSM-5. With a same probe molecule pyridine, a FTIR differential spectrum method was developed to identify the type and origin of the acid sites and their dependence on the temperature. An ITPD method was then used to analyze the TPD spectrum to describe the strength and amount of the acid sites according to the DAE of different segments.

2. Theoretical section

If no interactions exist between the adsorbed molecules, and the desorption is irreversible, the rate of desorption from a set of sites with a uniform DAE, E, is then given by Arrhenius law,

$$\frac{-\mathrm{d}(q_\mathrm{E})}{\mathrm{d}t} = k_\mathrm{E} \exp\left[\frac{-E}{RT}\right] q_\mathrm{E} \tag{1}$$

in which q_E (mol) is the amount of molecules desorbed with a definite E (J mol^{-1}). k_E (s^{-1}) is a pre-exponential factor, R the ideal gas constant (8.314 (J (mol K)$^{-1}$)) and T (K) the absolute temperature. The heating program here is such that the temperature increases linearly with time,

$$T = T_0 + \lambda t \tag{2}$$

Substituting Eq. (2) into Eq. (1) and taking logarithm of the resulting equation, we have,

$$\ln\left(\frac{-\mathrm{d}(q_\mathrm{E})}{\mathrm{d}T} \times \frac{\lambda}{q_\mathrm{E}}\right) = \ln k_\mathrm{E} - \frac{E}{RT} \tag{3}$$

By fitting the TPD data, Hashimoto et al. [38] applied Eq. (3) to calculate the values of k_E and E. They proposed also a relationship between k_E and E:

$$k_\mathrm{E} = \alpha \exp[\beta E] \tag{4}$$

where α (s^{-1}) and β (mol J^{-1}) are positive constants.

Masuda et al. [43] substituted Eqs. (2) and (4) into Eq. (1) and integrated the resulting differential equation which yielded Eq. (5).

$$\phi(E,T) = \frac{\Delta q}{\Delta q_0} = \exp\left[\frac{-\alpha e^{\beta E}}{a} \int_{T_0}^{T} \exp(-\frac{E}{RT})\,\mathrm{d}T\right] \tag{5}$$

During TPD, molecules desorb independently from a large number of sites, so that E can be expressed as a continuous distribution. Here, define $f(E)$ (mol^2 J^{-1}) as the distribution density function of the DAE. The number of sites with DAE between E and $E + \Delta E$ is proportional to $f(E)\,\mathrm{d}E$. The total amounts of the molecules initially adsorbed q_0 (mol) and remained q (mol) at temperature T on the sites are expressed as

$$q_0 = \int_0^\infty f(E)\,\mathrm{d}E \tag{6}$$

$$q = \int_0^\infty \phi(E,T)\, f(E)\,\mathrm{d}E \tag{7}$$

With simplification of Eq. (5), E and $f(E)$ are related to desorption temperature T by Eqs. (8) and (9) [43].

$$f(E) = \frac{(1+w)^2}{Ru\{(u+U/u)(e/2+w)+2U-u\}} \left(-\frac{\mathrm{d}q}{\mathrm{d}T}\right) \tag{8}$$

$$E = \frac{E_{in}(2w+e)}{\{2(w+1)\}} \tag{9}$$

The parameter E_{in} (J mol^{-1}), u, w and U are related to T by:

$$\frac{\lambda E_{in}}{(RT^2\alpha \exp[\beta E_{in}])} = \exp\left[\frac{-E_{in}}{(RT)}\right], \quad u = \frac{E_{in}}{(RT)},$$
$$w = u - \beta E_{in}, \quad U = \frac{2(u+2)}{(w+1)} \tag{10}$$

With Eqs. (8)–(10), at any T in the TPD spectrum, DAE can be calculated as long as α and β are determined. α and β can be obtained from the intercept and slope of the logarithm plot of k_E against E according to Eq. (4).

Masuda et al. [43] used Eqs. (8)–(10) to calculate the acid strength distribution as a function of the ammonia DAE. In this work the α and β values were calculated from the pyridine TPD profile of a ZSM-5 with Si/Al = 12.5 (ZSM5125).

The acid strength distribution can be divided into a finite number of intervals according to DAE. Acid sites in any interval are considered to have a same DAE. Then Eq. (7) is transformed into Eq. (11) which introduces a statistical concept of the acid strength.

$$q = \sum_{i=1}^{n} \phi(E,T)\, f(E_i) \Delta E_i \quad (n < \infty) \tag{11}$$

Considering that E and $f(E)$ are related to T. Eq. (11) is then written as Eq. (12):

$$q = \sum_{i=1}^{n} \varphi(T_i)\, \Delta T_i \quad (n < \infty) \tag{12}$$

$\varphi(T_i)$ is the distribution density function of desorption temperature and is assumed to present a uniform acid strength within a desorption temperature interval ΔT_i. $\varphi(T_i)$ is assumed to be Gaussian distribution and is represented by T_n which corresponds to the peak temperature of the distribution in the interval. $\varphi(T_i)$ can be determined through the differential spectra (DSs) between the two adjacent temperatures by the ITPD method [38]. It should be noted that the sites in an interval can be composed of different typed and originated acid sites, but a same DAE was assumed.

3. Experimental section

3.1. Zeolite sample

The ZSM5125 was supplied by Nanlian Institute of Sinopec Jinling Petrochemical Corporation. The sample was calcined at 823 K for 5 h according to the guidelines of the manufacturer to convert them directly to acidic form before use.

3.2. XRD and ^{27}Al NMR

Powder X-ray diffraction (XRD) pattern was measured using a Rigaku D/max 2500 v/pc automatic diffractometer. Solid-state ^{27}Al NMR spectrum was collected with a Varian Infinity plus 300 WB spectrometer, and at 78.1 MHz, with a pulse width of 0.6 μs, a pulse delay of 20 s, a spinning rate of 4 kHz.

3.3. FTIR

The samples were grounded into fine powders and pressed into very thin self supporting wafers with an optical diameter of 16 mm. The discs were mounted in a quartz IR cell equipped with a CaF_2 window and a vacuum system. Prior to adsorption, the samples were pretreated in situ at 673 K for 1.5 h under evacuation, then cooled to 398 K where pyridine vapor was introduced into the cell for 0.5 h. The physically adsorbed pyridine

was removed by evacuating for 1 h. After a spectrum was recorded, the sample was heated in vacuum for 1 h at 423, 473, 573 and 723 K stepwise, and a spectrum was recorded at each step. The spectrum of a clean sample was used for comparison and a Bruker vector 22 spectrometer was employed.

3.4. Pyridine TPD

TPD was carried out with a tubular stainless steel reactor at atmospheric pressure. 200 mg zeolite with particle size in 0.18–0.28 mm, crushed from tablets pressed at 130 MPa with the ZSM-5 powder without adding any binder. The system was quenched at 673 K for 1 h in a flow of He 40 ml min^{-1} (STP). After cooling to the prescribed temperature, pyridine was introduced with a pulsed injection with the He flow until saturation, indicated by the stabilization of the TCD signal. The sample was quenched again at the temperature for 2 h. Desorption was then performed under the same He flow with a ramp of 8 K min^{-1} to 823 K. Six starting temperatures were used for each sample, i.e. 398, 423, 448, 473, 498 and 723 K.

Demmin and Gorte [44] and Gorte [45] developed the criteria for testing the pore diffusion and readsorption effects in TPD experiments of porous materials. For the absence of gradients and readsorption within the particles, two equations should be satisfied.

$$\frac{QR_1}{4\pi R_1^2 N D_p} = \frac{Q\rho R_1^2}{3W_1 D_p} < 0.05 \quad (13)$$

$$\frac{\alpha\rho SFV(1-\varepsilon)}{Q} < 1 \quad (14)$$

where Q ($cm^3\ s^{-1}$) is the flow rate of carrier gas, R_1 (cm) the radius of the particles, N the number of particles in the bed, D_p ($cm^2\ s^{-1}$) the particle diffusion coefficient, ρ ($g\ cm^{-3}$) the particle density, W_1 (g) the weight of the sample, α ($cm^2\ g^{-1}$) the particle surface area, S the sticking coefficiency ($S < 1$), V (cm^3) the bed volume, ε the bed voidage ($\varepsilon < 1$), F ($cm\ s^{-1}$) the flow rate of gas to the surface and M the molecular weight of pyridine.

The sticking coefficiency of an aromatic molecule from gas phase to the catalytically active sites inside the channels of ZSM-5 is approximately 10^{-7} [46]. Since aromatic molecules and pyridine have similar molecular dimensions, these values can be used here. D_p is about 6×10^{-11} $cm^2\ s^{-1}$ for pyridine in ZSM-5 [47].

Here $\alpha\rho SFV(1-\varepsilon)/Q = 3.19 \times 10^6 \times S \times (1-\varepsilon) < 1$, $QR_1/4\pi R_1^2 ND_p = 0.013 < 0.05$. It can be assumed that the TPD experiment was carried out in the desorption controlled conditions.

4. Results

4.1. XRD and ^{27}Al NMR

The XRD pattern of the zeolite sample is shown in Fig. 1 which has only the peaks of ZSM-5. The ^{27}Al NMR spectrum of the sample is displayed in Fig. 2. The signal at around 50 ppm is ascribed to the tetrahedrally coordinated framework aluminum (Al_f) [48]. The resonance at around 0 ppm is due to the octahedrally coordinated extraframework aluminum (Al_{ef}) [49]. The major part of the aluminum exists as Al_f, however, the amount of Al_{ef} is significant.

4.2. FTIR

The IR spectrum of ZSM5125 consists of three major bands and three minor bands in the OH stretching region as shown in Fig. 3.

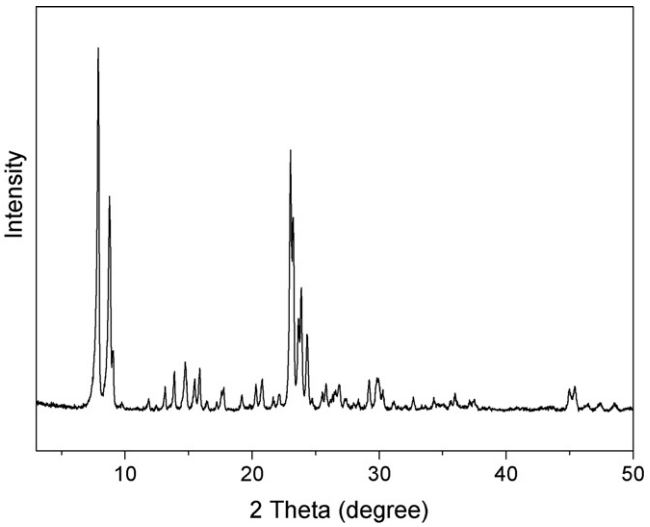

Fig. 1. X-ray diffraction pattern of the sample.

According to literature, the bands are assigned to different vibrations [40,50–55]. The band at 3600–3620 cm^{-1} is attributed to the framework bridged hydroxyl groups (AlOHSi). The one at 3660–3690 cm^{-1} is assigned to the extraframework AlOH groups ($AlOH_{ef}$s). The broad one at 3720–3740 cm^{-1} is associated with terminal silanol groups (SiOHs). Three less intense bands at ~3565, ~3630, ~3700 cm^{-1} are attributed to the H-bonded internal Si–OH, Si–OH nest, Si–OH H-bonded to $Si_x(OH)_y$, respectively [56–61]. Fig. 4 presents the evolution of the OH vibration bands versus the adsorption temperature measured with a stepwise increase, each step 1 h, of the temperature. After chemisorption at 398 K and removal of the physically adsorbed pyridine at the same temperature, the hydroxyl stretching bands at 3600–3620, 3660–3690 cm^{-1} disappeared completely. However, the band at 3720–3790 cm^{-1} did not disappear completely. After partly desorbed for 1 h at 423 K, the IR band at 3720–3790 cm^{-1} was restored. As the temperature increased stepwise from 423 to 473 K, the bands at 3600–3620 cm^{-1}, and 3660–3690 cm^{-1} rejuvenated. The intensities of the three bands did not increase further after the step of 573 K. The IR bands in hydroxyl stretching region after treatment at 723 K were obviously less intense than those at 573 K.

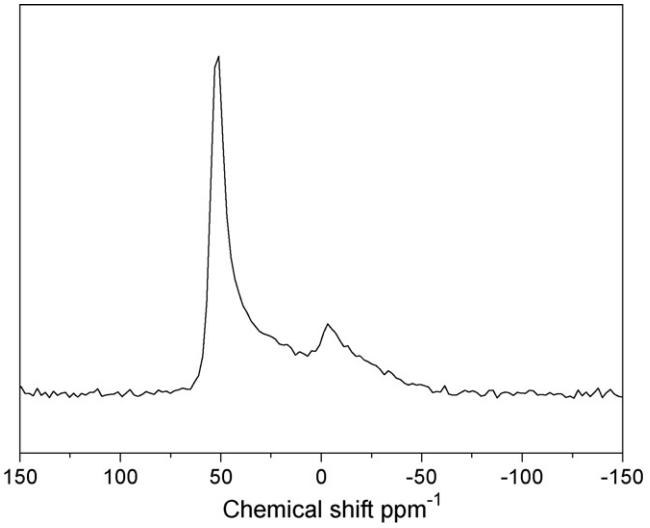

Fig. 2. ^{27}Al NMR spectrum.

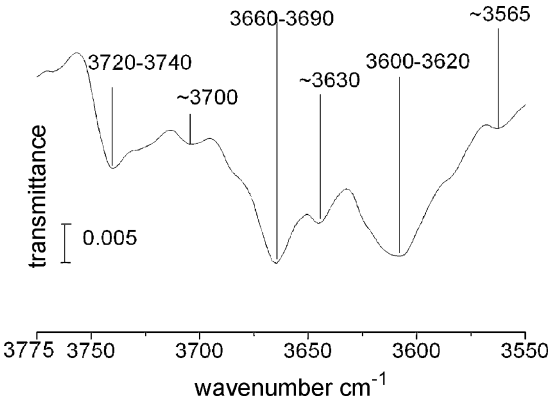

Fig. 3. FT-IR spectrum in the hydroxyl group stretching region (3775–3550 cm^{-1}) obtained after evacuation at 723 K.

Fig. 5(A) represents the variation of IR bands in 1425–1575 cm^{-1} region as the increase of the temperature. There are three bands in the region. The one at ~1450 cm^{-1} arising from the C–C stretch of a coordinatively bonded pyridine complex indicates the presence of L sites. The ~1540 cm^{-1} one is attributed to the C–C stretching vibration of the pyridinium ion and has been used for the identification of the B sites. The other at ~1490 cm^{-1} is attributed to the pyridine species interacting with both the two kinds of acid sites [62,63]. The DSs between those recorded at two adjacent temperatures are obtained and illustrated in Fig. 5(B). Fig. 5(A and B) shows that the intensity of the band at ~1450 cm^{-1} decreases quite fast and monotonically with the increase of temperature from 398 to 573 K, while that of the band at ~1540 cm^{-1} shows a complex profile with the increase of temperature. The intensity of the later shows an obvious reduction in temperature intervals of 398–423 and 573–723 K, and a minor change in 423–573 K. The intensity of the band at ~1490 cm^{-1} decreases monotonically with the increase of temperature.

4.3. Pyridine TPD

In order to determine the k_E and E, TPD spectra were measured by increasing the starting temperature, at which the sample was saturated by adsorption of pyridine and quenched consequently for 2 h, each time for 25 K (ΔT) from 398 to 523 K. The curves are shown in Fig. 6. For each temperature interval, the acid sites are assumed to have an identical strength and the amount of the sites is estimated by subtracting the two neighboring thermograms. The DSs of Fig. 6 are presented in Fig. 7. The areas below the curves represent the amount of acid sites with strength corresponding to an adsorption temperature range between T and $T + \Delta T$. Each of the curves in Fig. 7 is fitted with Eq. (3). k_E and E were estimated by non-linear least square regression and are listed in Table 1. The logarithm of k_E is plotted against E. The α, β of this material are estimated with Eq. (4) as 263 and 5.28×10^{-2}, respectively.

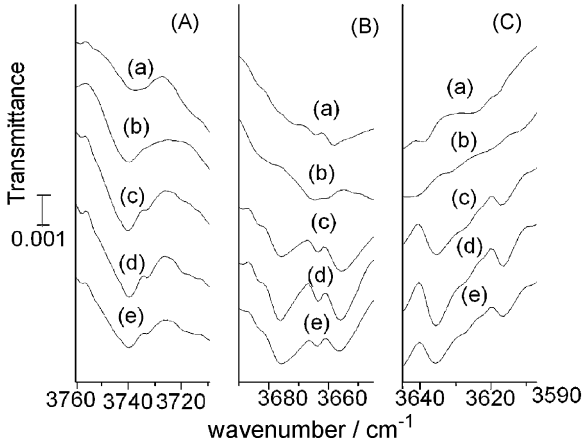

Fig. 4. FT-IR spectra in the hydroxyl group stretching region (A) 3760–3710 cm^{-1}, (B) 3690–3650 cm^{-1}, (C) 3645–3590 cm^{-1} obtained after adsorption of pyridine and desorption for 1 h at temperatures (a) 398 K, (b) 423 K, (c) 473 K, (d) 573 K, (e) 723 K.

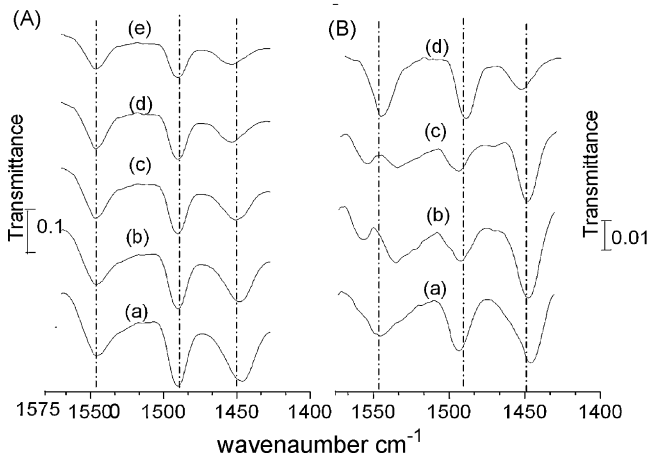

Fig. 5. FT-IR spectra. (A) Obtained after desorption of pyridine at different temperatures (a) 398 K, (b) 423 K, (c) 473 K, (d) 573 K, (e) 723 K in the region of 1570–1425 cm^{-1}. (B) Differential spectra corresponding to temperature ranges (a) 398–423 K, (b) 423–473 K, (c) 473–573 K, (d) 573–723 K.

5. Discussion

5.1. Purity of the sample

The XRD pattern shows that the sample is ZSM-5. However, as shown in Fig. 2, the ^{27}Al NMR spectrum shows that a considerable amount of Al_{ef} exists, which contributes to the extraframework acid sites within this context.

5.2. Type and origin of acid sites

The data presented in Fig. 4 indicate that a part of SiOHs are not B sits and do not adsorb pyridine, because the band of these groups

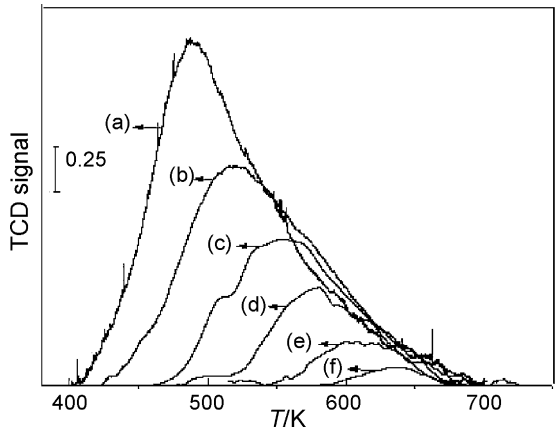

Fig. 6. Pyridine-TPD thermograms obtained by increasing the starting temperature from 398 to 573 K with 25 K steps. (a) 398 K, (b) 423 K, (c) 448 K, (d) 473 K, (e) 498 K, (f) 573 K.

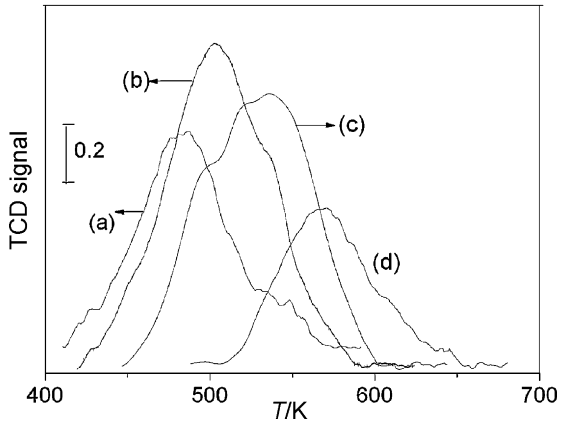

Fig. 7. Differential curves of pyridine-TPD thermograms between two adjacent starting temperatures in Fig. 4. (a) $\Delta T_{398-423\ K}$, (b) $\Delta T_{423-448\ K}$, (c) $\Delta T_{448-473\ K}$, (d) $\Delta T_{473-498\ K}$.

was not affected by pyridine adsorption. The B sites are recovered gradually with the stepwise increase of the desorption temperature. However, different bands, with different acid strength, recover at different temperatures. A general concept has been proposed that the lower the frequency, the stronger the acidity of the OH groups [64]. Here, the spectra in Fig. 4 do show a same trend, that the band at 3740 cm^{-1} recovered at lower temperature than the bands at 3600–3620 and 3660–3690 cm^{-1}. This means that the acid strength of AlOHSi and $AlOH_{ef}$ is stronger than the SiOHs.

In Fig. 5(A and B), the results indicate also the gradual rejuvenating of the acid sites as the increase of the desorption temperature. The areas under the IR bands at ~1540 and ~1450 cm^{-1} contain the information of the relative ratio of the B and L sites. The change of the ratio along with the adsorption temperature is informative. Fig. 5(B) shows that in the desorption temperature range 398–423 K both B and L sites are rejuvenated. However, the information in Fig. 4 shows only the reappearance of the SiOHs. Buzzoni et al. [51] proposed that the band at ~1540 cm^{-1} does not correspond to the pyridine adsorbed via hydrogen bond with SiOHs in zeolite, but corresponds more probably to that adsorbed with AlOHSis. However, Trombetta et al. [65] and Crépeau et al. [64] found respectively that a SiOHs group does interact with pyridine and exhibits an IR band with a wavenumber equivalent to that of the bridged groups. Trombetta et al. [65–67] found that the basic molecule adsorption caused the external terminal silanol group on ZSM-5 bridged with the vicinal Al cationic sites, as shown in Scheme 1. The data presented in Figs. 4 and 5 indicate that the acid sites associated with pyridine desorbed in a temperature range of 398–423 K are composed of both B and L sites, while the B sites are due to the SiOHs groups.

Fig. 5(B) shows that the intensity of the band at ~1450 cm^{-1} changes much, while that of the band at ~1540 cm^{-1} shows a minor change in between 423 and 473 K. It means that the B sites do not recover much in 423–473 K. However, in Fig. 4, it shows an

Table 1
E and K_E values estimated for four temperature intervals by fitting Eq. (1) with the TPD data of ZSM5125

T_0 (K)	$T_0 + \Delta T$ (K)	E (kJ mol^{-1})	K_E (s^{-1})
398	423	71.5	2.25×10^9
423	448	81.1	7.24×10^9
448	473	91.6	2.44×10^{10}
473	498	115.1	4.54×10^{11}

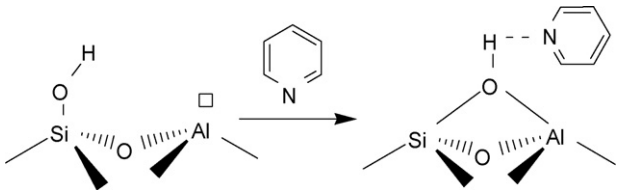

Scheme 1. Scheme of terminal silanol group geometry change induced by the adsorption of pyridine.

obvious increase of the intensity for the bands, i.e. ~3660–3690 cm^{-1} for the $AlOH_{ef}$s and ~3590–3640 cm^{-1} for the AlOHSis in 423–473 K. The ~1540 cm^{-1} band is associated with pyridine adsorbed on B sites which are the $AlOH_{ef}$s and the AlOHSis. It seems that the results in Figs. 4 and 5(B) have some inconsistency. This can be explained by the transformation of pyridinium ion dimmers (PyH...Py) to the pyridinium ions in this temperature interval. Crépeau et al. [64] postulated that pyridinium ion dimmers form due to the hydrogen bond interaction, as shown as Scheme 2. At a low temperature, e.g. 423 K, both the dimer and the ion coexist on the surface. The dimer decomposes to the pyridinium ion with enhancement of the band at ~1540 cm^{-1} and release of a pyridine molecule. At the same time, the independent ions decompose also according to Scheme 3 and lead to the rejuvenating of the bands in ~3660–3690 and ~3590–3640 cm^{-1} and the decrease of the band at ~1540 cm^{-1}. These processes result in a fact that the change of the band at ~1540 cm^{-1} in 423–473 K appears slower than in 398–423 and 573–723 K. Therefore, in 423–473 K both B and L sites are important and $AlOH_{ef}$s and the AlOHSis are associated with B sites.

In 473–573 K, consistent information is obtained from the data in Figs. 4 and 5. The spectra in hydroxyl region have no obvious change. The band at ~1450 cm^{-1} has a substantial change, while the band at ~1540 cm^{-1} keeps unchanged along with the temperature. Thus, it can be proposed that the acid sites with strength corresponding to pyridine desorption temperature 473–573 K are associated with L acidity.

Fig. 5 shows from 573 to 723 K, the ratio of B to L sites for desorption is the largest among all the temperature ranges examined. It is expected that an obvious increase of the bands intensities in the OH stretching region happened along with the decrease of the band intensity at ~1540 cm^{-1}. However, in Fig. 4 the intensities of the bands for hydroxyls are not increased, while the intensity of the band for AlOHSi decreased slightly along with the increase of the temperature. The evolution of OH stretching band observed with temperature above 673 K is similar to that observed by Auroux et al. [53] and Védrine et al. [62]. These authors explained that the dehydroxylation caused the decrease of the band intensity for OH stretching. It is then likely that the decomposition of pyridinium ion is accompanied with the dehydroxylation in this temperature range. It can be concluded that in the temperature range 573–723 K, B sites take the major role. According to the above mentioned analysis, the acid types and

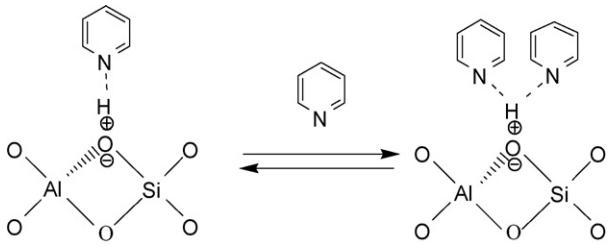

Scheme 2. The formation of pyridinium ion dimmers from pyridinium ion and its reverse.

Table 2
The acid types and origins of B sites for pyridine desorption in different temperature intervals

Temperature intervals	398–423 K	423–473 K	473–573 K	573–723 K
Acid type	B and L	B and L	L	B
Origin of B sites	SiOH groups	$AlOH_{ef}$s and the AlOHSis		

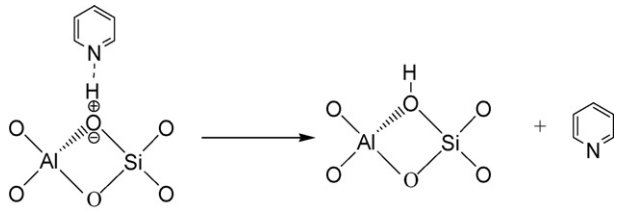

Scheme 3. The desorption of pyridinium ion into pyridine.

origins of B sites in different temperature intervals are identified and summarized in Table 2.

5.3. Acid strength distribution

According to the IR analysis, the TPD thermogram of pyridine on the sample was divided into four segments along the temperature scale, i.e. 398–423, 423–473, 473–573 and 573–723 K. The acid strength distribution of the sites desorbed pyridine within each segment was obtained from the DSs of Fig. 6 and was shown in Fig. 8. Based on the statistical concept of the acid strength distribution, each DS is assumed to correspond to a set of sites with a uniform acid strength. The DSs are almost Gaussian distribution and have their own peak temperatures, viz. 475, 500, 560, and 620 K. These temperatures are used to denote the corresponding set of sites. According to Eqs. (9) and (10), the DAE for the four sets are calculated as 70, 90, 120, and 150 kJ mol^{-1}, respectively. The results are in good agreement with that reported by Chen et al. [68]. They proposed that pyridine adsorption heats on B sites in zeolite are normally in a range 130–180 kJ mol^{-1} and that the lower adsorption heats are associated with the non-framework aluminum-containing species which may have both L and B acidity. Earlier work [39] proved that the pyridine DAE is almost the same as the pyridine adsorption heat.

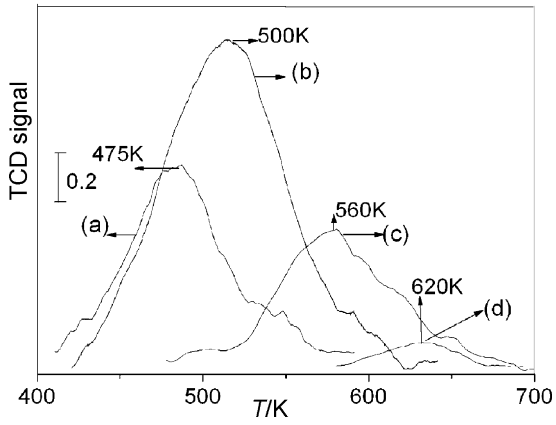

Fig. 8. Four sets of acid sites obtained from differential curves of pyridine-TPD thermograms between two adjacent starting temperatures in Fig. 4. (a) $\Delta T_{398\text{-}423\ K}$, (b) $\Delta T_{423\text{–}473\ K}$, (c) $\Delta T_{473\text{–}573\ K}$, (d) $\Delta T_{573\text{–}723\ K}$.

6. Conclusion

It has been demonstrated that with a comprehensive analysis of the pyridine TPD profile and FT-IR spectrum, detailed information on the amount, type, origination and strength distribution of the acid sites on ZSM-5 zeolite can be obtained. The acid type and hydroxyl structure corresponding to B sites in different temperature intervals were identified. In 398–423 K both B and L sites are important, and the B sites for desorption are associated with SiOHs. In 423–473 K, both B and L sites are important, but the B sites are mainly $AlOH_{ef}$s and AlOHSis. In 473–573 K, L sites are dominant, while in 573–723 K B sites take the major role. According to the result of IR analysis, the TPD thermogram of the sample was divided into four segments along the temperature scale. Based on the statistical concept of the acid strength distribution, the acid sites in the four segments were represented by different pyridine DAE, i.e. 70, 90, 120, and 150 kJ mol^{-1}, respectively.

Acknowledgements

This work has been supported by the Natural Science Foundation of China under contract number 20425619. The work has been also supported by the Program of Introducing Talents to the University Disciplines under file number B06006, and the Program for Changjiang Scholars and Innovative Research Teams in Universities under file number IRT 0641.

References

[1] J. Biswas, I.E. Maxwell, Appl. Catal. 58 (1990) 1.
[2] T. Yan, Ind. Eng. Chem. Proc. Des. Dev. 22 (1983) 154.
[3] I.E. Maxwell, Catal. Today 1 (1987) 385.
[4] N.Y. Chen, R.L. Gorring, H.R. Ireland, T.R. Stein, Oil Gas J. 75 (1977) 165.
[5] N.Y. Chen, J.L. Schlenker, W.E. Garwood, G.T. Kokotailo, J. Catal. 86 (1984) 24.
[6] J.G. Bendoraitis, A.W. Chester, F.G. Dewyer, W.E. Garwood, Stud. Surf. Sci. Catal. 28 (1986) 120.
[7] N.Y. Chen, J. Maziuk, A.B. Schwartz, P.B. Wiesz, Oil Gas J. 66 (1968) 154.
[8] N.Y. Chen, W.E. Garwood, W.O. Haag, A.B. Schwartz, Paper Presented at AIChE 72nd Annual Meeting, San Francisco, CA, (1979), p. 25.
[9] I.E. Maxwell, W.H.J. Stork, Stud. Surf. Sci. Catal. 137 (2001) 747.
[10] C.M.A.M. Mesters, D.G.R. Peferoen, J.P. Gilson, C. de Groot, P.T.M. van Brugge, K.P. de Jong, in: J. Weitkamp, B. Luecke (Eds.), Proceedings of the DGMK Conference on Solid Acids and Bases, Berlin, March 14–15, DGMK, Hamburg, 1996, p. 57.
[11] C.J. Maiden, Chemtech (1988) 38.
[12] S.A. Tabak, G.J. Weiss, Synfuels 4th Worldwide Symposium, Washington, DC, 1984.
[13] W.O. Haag, D.H. Olson, P.B. Weisz, in: Proceedings of the 29th IUPAC Congress, 1984, p. 327.
[14] J.S. Beck, W.O. Haag, in: G. Ertl, H. Knözinger, J. Weitkamp (Eds.), Handbook of Heterogeneous Catalysis, vol. 5, Wiley-VCH, Weinheim, 1997, p. 2123.
[15] S. Bhatia, Zeolite Catalysis: Principles and Application, CRC Press, Boca Raton, FL, 1990.
[16] X.C. Meng, Y.X. Wu, Y.D. Li, J. Porous Mater. 13 (2006) 365.
[17] H.J. Zhang, X.C. Meng, Y.D. Li, Y.S. Lin, Ind. Eng. Chem. Res. 46 (2007) 4186.
[18] H.R. Liu, X.C. Meng, D.S. Zhao, Y.D. Li, Chem. Eng. J. (2007), doi:10.1016/j.cej.2007.11.010.
[19] H.J. Zhang, Y.D. Li, Powder Technol. 183 (2008) 73.
[20] Y.M. Liu, H.Q. Yang, F. Jin, Y. Zhang, Y.D. Li, Chem. Eng. J. 136 (2008) 282.
[21] H.Q. Yang, Y.M. Liu, Y.D. Li, J. Mol. Catal. (China) 20 (2006) 477.
[22] A.W. Smith, F. Anoff, J. Phys. Chem. 62 (1958) 684.
[23] R.J. Cvetović, Y. Amenomiya, Adv. Catal. 17 (1967) 103.
[24] R.J. Cvetović, Y. Amenomiya, Catal. Rev. Sci. Eng. 6 (1972) 21.
[25] J.A. Konvalinka, J.J.F. Scholten, J.C. Rasser, J. Catal. 48 (1977) 365.
[26] B. Hunger, J. Hoffmann, Thermochim. Acta 106 (1986) 133.

[27] L. Forni, E. Magni, J. Catal. 112 (1988) 437.
[28] K.J. Leary, J.N. Michaels, A.M. Stacy, AIChE J. 34 (1988) 263.
[29] J.L. Lemaitre, in: F. Delannay (Ed.), Characterization of Heterogeneous Catalysts, Marcel Dekker Press, New York and Basel, 1990, p. 29.
[30] M. Sawa, M. Niwa, Y. Murakami, Zeolites 10 (1990) 307.
[31] S. Bhatia, J. Beltramini, D.D. Do, Catal. Today 7 (1990) 309.
[32] J.L. Falconer, R.J. Madix, J. Catal. 48 (1977) 262.
[33] S.R. Yang, Chin. J. Catal. 4 (1983) 57.
[34] W.R. Xu, Y.G. Tao, S.R. Yang, Chin. J. Catal. 14 (1993) 77.
[35] X. Duan, Q. Wang, Chin. J. Catal. 7 (1986) 169.
[36] M. Sawa, M. Niwa, Y. Murakami, Zeolites 11 (1991) 93.
[37] N. Katada, H. Igi, J.H. Kim, M. Niwa, J. Phys. Chem. B 101 (1997) 5969.
[38] K. Hashimoto, T. Masuda, T. Mori, Stud. Surf. Sci. Catal. 28 (1986) 503.
[39] J.A. Schwarz, B.J. Russell, H.F. Harnsberger, J. Catal. 54 (1978) 303.
[40] N.Y. Topsøe, K. Pedersen, E.G. Derouane, J. Catal. 70 (1981) 41.
[41] J.A. Lercher, G. Ritter, H. Vinek, J. Colloid Interface Sci. 106 (1985) 215.
[42] T. Kawai, K.M. Jiang, T. Ishikawa, J. Catal. 159 (1996) 288.
[43] T. Masuda, Y. Fujikata, H. Ikeda, S. Matsushita, K. Hashimoto, Appl. Catal. A: Gen. 162 (1997) 29.
[44] R.A. Demmin, R.J. Gorte, J. Catal. 90 (1984) 32.
[45] R.J. Gorte, J. Catal. 75 (1984) 164.
[46] H. Tanakaa, S. Zhenga, A. Jentysa, J.A. Lerchera, Stud. Surf. Sci. Catal. 142 (2002) 1619.
[47] H. Bludau, H.G. Karge, W. Niessen, Micropor. Mesopor. Mater. 22 (1998) 297.
[48] M. Sawa, M. Niva, Y. Murakami, Zeolites 10 (1990) 532.
[49] J. Klinowski, J.M. Thomas, C.A. Fyfe, G.C. Gobbi, J.S. Hartman, Inorg. Chem. 22 (1983) 63.
[50] A. Maiganen, E.G. Derouane, J.B. Nagy, Appl. Surf. Sci. 75 (1994) 204.
[51] R. Buzzoni, S. Bordiga, G. Ricchiardi, C. Lamberti, Langmuir 12 (1996) 930.
[52] S. Kotrel, M.P. Rosynek, J.H. Lunsford, J. Catal. 182 (1999) 278.
[53] B.A. Auroux, V. Bolis, P. Weerzchowski, P.C. Gravelle, J.C. Védrine, J. Chem. Soc. Farad. Trans. I 75 (1979) 2544.
[54] M. Trombetta, T. Armarol, A.G. Alejandre, Appl. Catal. A: Gen. 192 (2000) 125.
[55] A. Ungureanu, T.V. Hoang, D. Trongon, Appl. Catal. A: Gen. 294 (2005) 92.
[56] J.W. Ward, J. Catal. 9 (1967) 225.
[57] P.A. Jacobs, W.J. Mortier, Zeolites 2 (1982) 226.
[58] A. Zecchina, S. Bordiga, G. Spoto, D. Scarano, G. Petrini, G. Leofanti, M. Padovan, C. Otero Areàn, J. Chem. Soc. Farad. Trans. I 88 (1992) 2959.
[59] U. Lohse, E. Leffler, M. Hunger, J. Steckner, V. Patzelová, Zeolites 7 (1987) 11.
[60] O. Cairon, K. Thomas, T. Chevreau, Micropor. Mesopor. Mater. 46 (2001) 327.
[61] I. Halasz, M. Agarwal, B. Marcus, W.E. Cormier, Micropor. Mesopor. Mater. 84 (2005) 318.
[62] J.C. Védrine, A. Auroux, V. Bolis, P. Dejaifve, C. Naccache, P. Wierzchowski, E.G. Derouane, J.B. Nagy, J.P. Gilson, J.H.C. van Hooff, J.P. van den Berg, J. Wolthuizen, J. Catal. 59 (1979) 248.
[63] A. Maijanen, E.G. Derouane, J.B. Nagy, Appl. Surf. Sci. 75 (1994) 204.
[64] G. Crépeau, V. Montouillout, A. Vimont, L. Mariey, T. Cseri, F. Mauge, J. Phys. Chem. B 10 (2006) 15172.
[65] M. Trombetta, G. Busca, S. Rossini, V. Piccoli, V. Piccoli, U. Cornaro, Y.A. Guercio, R. Catani, R.J. Willeyz, J. Catal. 179 (1998) 581.
[66] M. Trombetta, G. Busca, J. Catal. 187 (1999) 521.
[67] M. Trombetta, T. Armaroli, A.G. Alejandre, J.R. Solis, G. Busca, Appl. Catal. A: Gen. 192 (2000) 125.
[68] D.T. Chen, S. Sharma, N. Cardona-Martinez, J.A. Dumesic, V.A. Bell, G.D. Hodge, R.J. Madon, J. Catal. 136 (1992) 392.